

## Article

# A New Approach for Analyzing Circular Tunnels in Nonlinear Strain-Softening Rock Masses Considering Seepage Force

Hao Fan, Lei Wang \* and Shaobo Li 

State Key Laboratory of Mining Response and Disaster Prevention and Control in Deep Coal Mines, Anhui University of Science and Technology, Huainan 232001, China

\* Correspondence: leiwang723@126.com; Tel.: +86-0554-6631588

**Abstract:** Accurate calculation of the stresses and deformations of tunnels is of great importance for practical engineering applications. In this study, a three-region model for tunnels considering seepage force was established. A new nonlinear strain-softening model is proposed. Then, a unified solution for the stresses and deformations of tunnels is deduced. Through a series of discussions, the effects of seepage force, softening modulus coefficient of cohesion, and initial support resistance on the stress distribution, radii of the post-peak zone, and surface displacement around the tunnel are discussed. Results show that the tangential stresses are always larger than the radial stresses. As the distance from the tunnel center increases, the radial stress continues to increase, while the tangential stress first increases and then decreases. With the increases in seepage force, the radii of the post-peak zone and surface displacement all increase. With the increases in softening modulus coefficient of cohesion, the radii of the post-peak zone increase while the surface displacement decreases. Tunnels with a higher initial support resistance experience lower radii of the post-peak zone and surface displacement.

**Keywords:** tunnel; stresses and deformations; nonlinear strain-softening; seepage force



**Citation:** Fan, H.; Wang, L.; Li, S. A New Approach for Analyzing Circular Tunnels in Nonlinear Strain-Softening Rock Masses Considering Seepage Force. *Minerals* **2023**, *13*, 138. <https://doi.org/10.3390/min13020138>

Academic Editor: Yosoon Choi

Received: 11 December 2022

Revised: 8 January 2023

Accepted: 16 January 2023

Published: 17 January 2023



**Copyright:** © 2023 by the authors. Licensee MDPI, Basel, Switzerland. This article is an open access article distributed under the terms and conditions of the Creative Commons Attribution (CC BY) license (<https://creativecommons.org/licenses/by/4.0/>).

## 1. Introduction

With the rapid development of society and the economy, many huge infrastructure projects have been put into construction. As one of the most common structures, tunnels are widely used in water conservancy engineering and underground traffic engineering [1–3]. The stress state in the underground rock will change after the excavation of tunnels [4,5]. Once the changed stress exceeds the ultimate strength of the rock mass, the tunnel surrounding the rock would be destroyed, and three different regions (a damaged region, a strain-softening region, and an elastic region) would be formed, which would exert a significant impact on the stability of the tunnel [6–10]. Therefore, accurate stress analysis of the surrounding rock is very important to the stability control of the tunnel.

The appropriate constitutive models for different types of rock materials are the key to solving the stresses and deformation of tunnels. In past decades, the elastic–brittle–plastic constitutive model (Figure 1a), suitable for hard rock masses with Geological Strength Index (GSI) values above 75, and the elastic–perfectly plastic constitutive model (Figure 1b) for soft rock masses with GSI values below 25, were usually used to research this problem [11–16]. However, the strain-softening behavior of rock mass was ignored by the first two constitutive models. The third model, called the linear strain-softening constitutive model (Figure 1c), considering the linear deterioration of strength parameters in the strain-softening region, can stand for a wider range of rock masses with  $25 < \text{GSI} < 75$  [17–20]. Moreover, the elastic–perfectly plastic constitutive model (the slope of the strain-softening stage is equal to null) and the elastic–brittle–plastic constitutive model (the slope of the strain-softening stage is equal to infinity) are both special cases of the linear strain-softening constitutive model. In fact, the mechanical parameters of rock mass, such as cohesion, tend to decrease nonlinearly in the post-peak stage [21,22]. Thus, the nonlinear strain-softening

constitutive model (Figure 1d) was presented and selected as the constitutive model for the rock mass in this study.

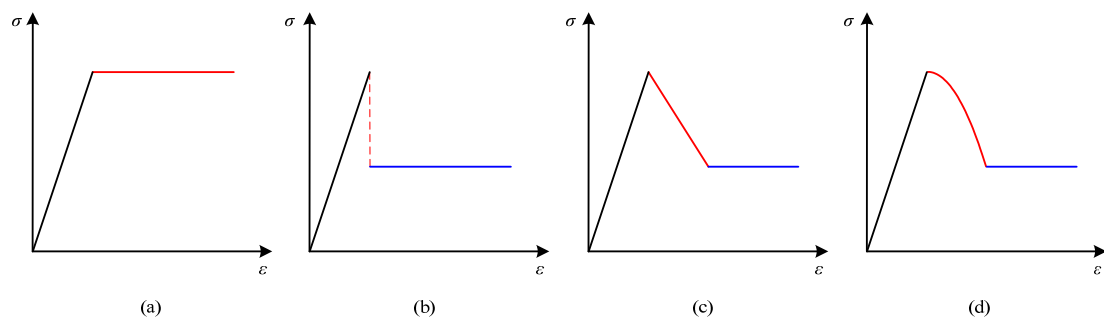


**Figure 1.** Different constitutive models. (a) elastic–perfectly plastic; (b) elastic–brittle-plastic; (c) linear strain-softening; (d) nonlinear strain-softening.

Groundwater is one of the important components of underground engineering structures. The seepage force caused by the flow of groundwater also has a non-negligible influence on the stress state around the tunnel [23–25]. Therefore, the seepage force is expected to be taken into consideration in the theoretical analysis of tunnels. In order to accurately analyze the stresses and deformations of tunnels in nonlinear strain-softening rock masses considering seepage force. In the present study, a mechanical model for tunnels in water-rich areas is established. A new nonlinear strain-softening model that considers the nonlinear degradation of cohesion is proposed. Based on the Mogi–Coulomb criterion, a unified solution for the stresses and displacements of the surrounding rock is determined. Through a series of case studies, the effects of seepage force, softening modulus coefficient of cohesion, and initial support resistance on the stress distribution, radii of the post-peak region, and surface displacement around the tunnel are discussed.

### 2. Model Establishment

As shown in Figure 2, assuming that there is a cylindrical tunnel in the water-rich area and the surrounding rock is a nonlinear strain-softening media, the original in-situ stress is  $\sigma_0$ . After the tunnel excavation and stress redistribution, a crushed region, strain-softening region, and elastic region were formed in the surrounding rock around the tunnel. The radii of the tunnel and the three regions are sequentially recorded as  $R_0$ ,  $R_c$ ,  $R_s$ , and  $R_e$ . In addition, an initial support resistance ( $P_i$ ) was uniformly applied to the excavation surface to maintain the stability of the tunnel.

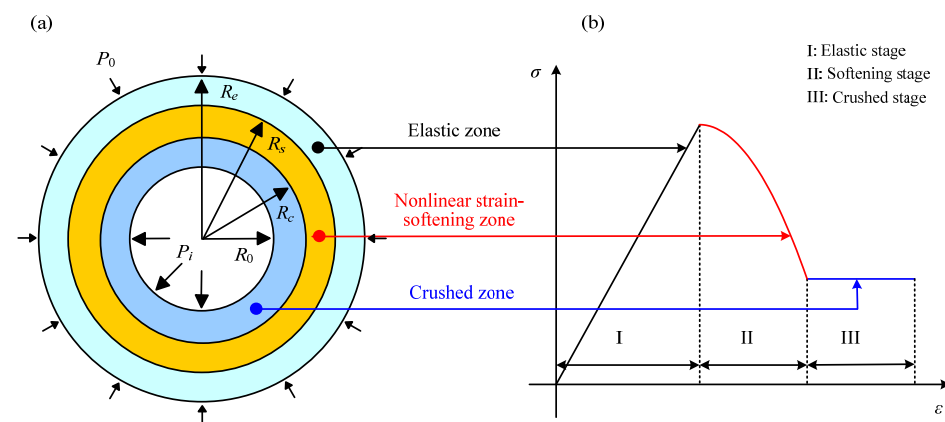


**Figure 2.** Mechanical models. (a) Three-region model of a tunnel cylindrical considering seepage force. (b) Nonlinear strain-softening model of surrounding rock.

We assume that the seepage force is evenly distributed outside the elastic region of the tunnel. Based on Darcy’s law, the differential equation for the seepage force is given by the following equation:

$$\frac{d^2 P_w}{dr^2} + \frac{1}{r} \frac{dP_w}{dr} = 0 \tag{1}$$

where  $P_w$  is the seepage force anywhere around the tunnel.

Combining the boundary conditions,  $P_w = 0, r = R_0$  and  $P_w = P_0, r = R_e$ , the seepage force can be solved as

$$P_w = P_0 \frac{\ln(R_0/r)}{\ln(R_0/R_e)} \tag{2}$$

Generally, the cohesion in the strain-softening region decreases nonlinearly, and the softening modulus of cohesion increases with the increase in strain, as shown in Figure 3. We assume that the softening modulus of cohesion is as follows:

$$E' = \alpha \varepsilon_\theta \tag{3}$$

where  $\alpha$  is the softening modulus coefficient of cohesion, which reflects the brittleness of the rock mass. The rock mass is ideal elastic-strain-softening when  $\alpha = 0$ , and the greater the softening coefficient, the more brittle the rock.

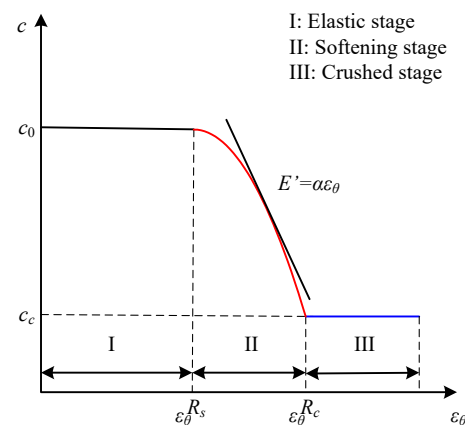


Figure 3. Nonlinear strain-softening model of cohesion.

### 3. Mechanical Analysis

To solve the three-region model shown in Figure 1, the following basic formulas should be given as [26,27]:

1. Equilibrium differential formula:

$$\frac{d\sigma_r}{dr} + \frac{\sigma_r - \sigma_\theta}{r} + \eta \frac{dP_w}{dr} = 0 \tag{4}$$

where  $\sigma_r$  and  $\sigma_\theta$  are the radial and tangential stresses, respectively, and  $\eta$  is the seepage force coefficient.

2. Geometric formula:

$$\begin{cases} \varepsilon_r = \frac{du}{dr} \\ \varepsilon_\theta = \frac{u}{r} \end{cases} \tag{5}$$

where  $\varepsilon_r$  and  $\varepsilon_\theta$  are the radial and tangential strains, respectively.

3. Constitutive formula:

$$\begin{cases} \varepsilon_r = \frac{1 - \mu^2}{E} \left( \sigma_r - \frac{\mu}{1 - \mu} \sigma_\theta \right) \\ \varepsilon_\theta = \frac{1 - \mu^2}{E} \left( \sigma_\theta - \frac{\mu}{1 - \mu} \sigma_r \right) \end{cases} \quad (6)$$

where  $E$  is the elastic modulus of rock mass, and  $\mu$  is the Poisson’s ratio of rock mass.

4. Mogi-Coulomb strength criterion:

$$\sigma_\theta = M\sigma_r + N \quad (7)$$

where  $M = (\sqrt{3} + 2 \sin \varphi) / (\sqrt{3} - 2 \sin \varphi)$  and  $N = 4c \cos \varphi / (\sqrt{3} - 2 \sin \varphi)$ .

### 3.1. Stresses and Displacement in the Elastic Region

By substituting Equations (2), (5), and (6) into Equation (4), the following differential equation of the displacement in the elastic region can be deduced:

$$\frac{d^2 u_e}{dr^2} + \frac{1}{r} \frac{du_e}{dr} - \frac{u_e}{r^2} = \frac{\eta F v}{r E} \quad (8)$$

where  $v = \frac{(1 + \mu)(1 - 2\mu)}{1 - \mu}$  and  $F = P_0 / (\ln(R_0/R_e))$ .

Solving Equation (8), we can obtain

$$u_e = C_1 r + \frac{C_2}{r} + \frac{\eta F v r \ln r}{2E} \quad (9)$$

where  $C_1$  and  $C_2$  are undetermined constants.

By substituting Equation (9) into Equation (5), the following strains can be deduced:

$$\begin{cases} \varepsilon_{re} = C_1 - \frac{C_2}{r^2} + \frac{\eta F v}{2E} (\ln r + 1) \\ \varepsilon_{\theta e} = C_1 + \frac{C_2}{r^2} + \frac{\eta F v \ln r}{2E} \end{cases} \quad (10)$$

where  $C_1$  and  $C_2$  are undetermined constants.

By integrating Equations (6) and (10), we can obtain the radial and tangential stresses:

$$\begin{cases} \sigma_{re} = \frac{EC_1}{(1 + \mu)(1 - 2\mu)} - \frac{EC_2}{(1 + \mu)r^2} + \frac{\eta F \ln r}{2(1 - \mu)} + \frac{\eta F}{2} \\ \sigma_{\theta e} = \frac{EC_1}{(1 + \mu)(1 - 2\mu)} + \frac{EC_2}{(1 + \mu)r^2} + \frac{\eta F \ln r}{2(1 - \mu)} + \frac{\mu \eta F}{2(1 - \mu)} \end{cases} \quad (11)$$

With the stress boundary conditions  $\sigma_r = \sigma_r^{e-s}$ ,  $r = R_s$  and  $\sigma_r = \sigma_0 + P_0$  at  $r = R_e$ ,  $C_1$  and  $C_2$  can be deduced as follows:

$$\begin{cases} C_1 = \frac{v(1 - \mu)}{E} (\sigma_0 + P_0) + \frac{R_s^2}{R_e^2 - R_s^2} \frac{v(1 - \mu)}{E} (\sigma_0 + P_0 - \sigma_r^{e-s}) + \frac{\eta F v}{2E} \frac{R_s^2}{R_e^2 - R_s^2} \ln \frac{R_s}{R_e} - \frac{\eta F v (1 - \mu)}{2E} - \frac{\eta F v}{2E} \ln R_e \\ C_2 = \frac{1 + \mu}{E} \frac{R_e^2 R_s^2}{R_e^2 - R_s^2} (\sigma_0 + P_0 - \sigma_r^{e-p}) + \frac{\eta F (1 + \mu)}{2E(1 - \mu)} \frac{R_e^2 R_s^2}{R_e^2 - R_s^2} \ln \frac{R_s}{R_e} \end{cases} \quad (12)$$

By substituting Equation (12) into Equation (11), the stresses in the elastic region can be solved:

$$\begin{cases} \sigma_{re} = \sigma_0 + P_0 + \frac{\eta F}{2(1 - \mu)} \ln \frac{r}{R_e} + \frac{R_s^2}{R_s^2 - R_e^2} \left( \frac{R_e^2}{r^2} - 1 \right) \left[ \sigma_0 + P_0 - \sigma_r^{e-s} + \frac{\eta F}{2(1 - \mu)} \ln \frac{R_s}{R_e} \right] \\ \sigma_{\theta e} = \sigma_0 + P_0 + \frac{\eta F \ln(r/R_e) + 2\mu - 1}{2(1 - \mu)} - \frac{R_s^2}{R_s^2 - R_e^2} \left( \frac{R_e^2}{r^2} + 1 \right) \left[ \sigma_0 + P_0 - \sigma_r^{e-s} + \frac{\eta F}{2(1 - \mu)} \ln \frac{R_s}{R_e} \right] \end{cases} \quad (13)$$

The radial and tangential stresses should satisfy Equation (7) at  $r = R_s$ , so we can obtain

$$\sigma_r^{e-s} = \frac{-2R_e^2(\sigma_0 + P_0) + \frac{\eta F}{2(1-\mu)} \left[ (R_s^2 - R_e^2) \left( \ln \frac{R_s}{R_e} + 2\mu - 1 \right) - (R_s^2 + R_e^2) \ln \frac{R_s}{R_e} \right] - N_e(R_s^2 - R_e^2)}{M(R_s^2 - R_e^2) - R_s^2 - R_e^2} \quad (14)$$

By substituting Equation (11) into Equation (6), the radial and tangential strains in the elastic region can be deduced:

$$\begin{cases} \varepsilon_{re} = C_1 - \frac{C_2}{r^2} + \frac{\eta F v}{2E} (\ln r + 1) \\ \varepsilon_{\theta e} = C_1 + \frac{C_2}{r^2} + \frac{\eta F v \ln r}{2E} \end{cases} \quad (15)$$

Combining with Equations (5) and (15), the displacement in the elastic region can be derived:

$$u_e = C_1 r + \frac{C_2}{r} + \frac{\eta F v r \ln r}{2E} \quad (16)$$

### 3.2. Stresses and Displacement in the Strain-Softening Region

Generally, the volume of roadway surrounding rock will expand after exaction. The relationship between the dilation coefficient and strains is shown in Figure 4.

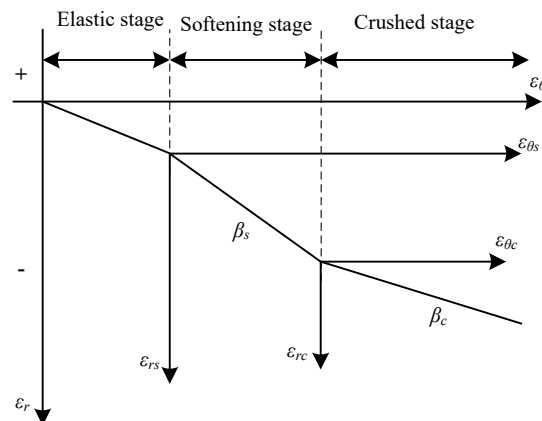


Figure 4. Dilation model of rock mass.

According to the non-associated flow law, the relationship between radial and tangential strains in strain-softening and crushed regions can be denoted as

$$\begin{cases} \varepsilon_{rs} + \beta_s \varepsilon_{\theta s} = 0 \\ \varepsilon_{rc} + \beta_c \varepsilon_{\theta c} = 0 \end{cases} \quad (17)$$

where  $\beta_s$  and  $\beta_c$  are the dilation coefficient in strain-softening and crushed regions, respectively. They can be obtained by

$$\begin{cases} \beta_s = \frac{1 + \sin \psi_s}{1 - \sin \psi_s} \\ \beta_c = \frac{1 + \sin \psi_c}{1 - \sin \psi_c} \end{cases} \quad (18)$$

where  $\psi_s$  and  $\psi_c$  are the dilation angle in strain-softening and crushed regions, respectively.

The total strains consist of elastic and strain-softening parts in the strain-softening region:

$$\begin{cases} \varepsilon_r = \varepsilon_{rs} + \varepsilon_r^{e-s} \\ \varepsilon_{\theta} = \varepsilon_{\theta s} + \varepsilon_{\theta}^{e-s} \end{cases} \quad (19)$$

where  $\epsilon_r^{e-s}$  and  $\epsilon_\theta^{e-s}$  are the radial and tangential strains on the interface between the elastic and strain-softening regions, respectively.

By integrating Equations (5), (17), and (19), the differential equation for displacement in the strain-softening region can be deduced:

$$\frac{du_s}{dr} + \beta_s \frac{u_s}{r} = \epsilon_r^{e-s} + \beta_s \epsilon_\theta^{e-s} \tag{20}$$

When  $u_s = u^{e-s}$  and  $r = R_s$ , Equation (20) can be solved:

$$u_s = \left[ \frac{u^{e-s} - \epsilon_r^{e-s} R_s}{\beta_s + 1} \right] \left( \frac{R_s}{r} \right)^{\beta_s} + \frac{(\epsilon_r^{e-s} + \beta_s \epsilon_\theta^{e-s}) r}{\beta_s + 1} \tag{21}$$

The strains in the strain-softening region can be deduced by substituting Equation (21) into Equation (5):

$$\begin{cases} \epsilon_{rs} = \frac{\beta_s(\epsilon_r^{e-s} - \epsilon_\theta^{e-s})}{\beta_s + 1} \left( \frac{R_s}{r} \right)^{\beta_s+1} + \frac{\epsilon_r^{e-s} + \beta_s \epsilon_\theta^{e-s}}{\beta_s + 1} \\ \epsilon_{\theta s} = \frac{\epsilon_\theta^{e-s} - \epsilon_r^{e-s}}{\beta_s + 1} \left( \frac{R_s}{r} \right)^{\beta_s+1} + \frac{\epsilon_r^{e-s} + \beta_s \epsilon_\theta^{e-s}}{\beta_s + 1} \end{cases} \tag{22}$$

As shown in Figure 2b, the cohesion in the nonlinear strain-softening region can be written as

$$\begin{aligned} c_s &= c_0 - \alpha \epsilon_{\theta s} (\epsilon_{\theta s} - \epsilon_\theta^{e-s}) \\ &= c_0 - \alpha \left[ \frac{\epsilon_\theta^{e-s} - \epsilon_r^{e-s}}{\beta_s + 1} \left( \frac{R_s}{r} \right)^{\beta_s+1} + \frac{\epsilon_r^{e-s} + \beta_s \epsilon_\theta^{e-s}}{\beta_s + 1} \right] \left[ \frac{\epsilon_\theta^{e-s} - \epsilon_r^{e-s}}{\beta_s + 1} \left( \frac{R_s}{r} \right)^{\beta_s+1} + \frac{\epsilon_r^{e-s} + \beta_s \epsilon_\theta^{e-s}}{\beta_s + 1} - \epsilon_\theta^{e-s} \right] \\ &= c_0 - \frac{\alpha(\epsilon_\theta^{e-s} - \epsilon_r^{e-s})}{\beta_s + 1} \left[ \frac{\epsilon_\theta^{e-s} - \epsilon_r^{e-s}}{\beta_s + 1} \left( \frac{R_s}{r} \right)^{2(\beta_s+1)} + \frac{2\epsilon_r^{e-s} + (\beta_s - 1)\epsilon_\theta^{e-s}}{\beta_s + 1} \left( \frac{R_s}{r} \right)^{\beta_s+1} - \frac{\epsilon_r^{e-s} + \beta_s \epsilon_\theta^{e-s}}{\beta_s + 1} \right] \end{aligned} \tag{23}$$

where  $c_0$  is the initial cohesion.

By substituting Equations (2), (7) and (23) into Equation (4), the differential equation for the radial stress in the strain-softening region can be deduced:

$$\frac{d\sigma_r}{dr} + \frac{(1-M)\sigma_r}{r} + \frac{A \left( \frac{R_s}{r} \right)^{2(\beta_s+1)} + B \left( \frac{R_s}{r} \right)^{\beta_s+1} - D}{r} - \frac{N_e + \eta F}{r} = 0 \tag{24}$$

where

$$\begin{cases} A = \frac{4 \cos \varphi \alpha (\epsilon_\theta^{e-s} - \epsilon_r^{e-s})^2}{(\sqrt{3} - 2 \sin \varphi) (\beta_p + 1)^2} \\ B = \frac{4 \cos \varphi \alpha (\epsilon_\theta^{e-s} - \epsilon_r^{e-s}) (\beta_p \epsilon_\theta^{e-s} - \epsilon_\theta^{e-s} + 2\epsilon_r^{e-s})}{(\sqrt{3} - 2 \sin \varphi) (\beta_s + 1)^2} \\ D = \frac{4 \cos \varphi \alpha (\epsilon_\theta^{e-s} - \epsilon_r^{e-s}) (\epsilon_r^{e-s} + \beta_s \epsilon_\theta^{e-s})}{(\sqrt{3} - 2 \sin \varphi) (\beta_s + 1)^2} \end{cases} \tag{25}$$

When  $r = R_s$  and  $\sigma_r = \sigma_r^{e-s}$ , the stresses in the strain-softening region can be solved:

$$\left\{ \begin{aligned} \sigma_{rs} &= \left( \sigma_r^{e-s} - \frac{N_e + \eta F + D}{1 - M} \right) \left( \frac{R_s}{r} \right)^{1-M} - \frac{A}{2\beta_s + M + 1} \left[ \left( \frac{R_s}{r} \right)^{1-M} - \left( \frac{R_s}{r} \right)^{2(\beta_s+1)} \right] - \\ &\quad \frac{B}{\beta_s + M} \left[ \left( \frac{R_s}{r} \right)^{1-M} - \left( \frac{R_s}{r} \right)^{\beta_s+1} \right] + \frac{N_e + \eta F + D}{1 - M} \\ \sigma_{\theta s} &= M \left\{ \left( \sigma_r^{e-s} - \frac{N_e + \eta F + D}{1 - M} \right) \left( \frac{R_s}{r} \right)^{1-M} - \frac{A}{2\beta_s + M + 1} \left[ \left( \frac{R_s}{r} \right)^{1-M} - \left( \frac{R_s}{r} \right)^{2(\beta_s+1)} \right] - \frac{B}{\beta_s + M} \cdot \right. \\ &\quad \left. \left[ \left( \frac{R_s}{r} \right)^{1-M} - \left( \frac{R_s}{r} \right)^{\beta_s+1} \right] + \frac{N_e + \eta F + D}{1 - M} \right\} + N_e - A \left( \frac{R_s}{r} \right)^{2(\beta_s+1)} - B \left( \frac{R_s}{r} \right)^{\beta_s+1} + D \end{aligned} \right. \quad (26)$$

### 3.3. Stresses and Displacement in the Crushed Region

The total strains consist of strain-softening and crushed parts in the crushed region and we can obtain

$$\begin{cases} \epsilon_r = \epsilon_{rc} + \epsilon_r^{s-c} \\ \epsilon_\theta = \epsilon_{\theta c} + \epsilon_\theta^{s-c} \end{cases} \quad (27)$$

where  $\epsilon_r^{s-d}$  and  $\epsilon_\theta^{s-d}$  are the radial and tangential strains at  $r = R_c$ , respectively.

By integrating Equations (5), (17), and (27), the differential equation for the displacement in the crushed region can be deduced:

$$\frac{du_c}{dr} + \beta_c \frac{u_c}{r} = \epsilon_r^{s-c} + \beta_c \epsilon_\theta^{s-c} \quad (28)$$

When  $r = R_c$  and  $u_c = u^{s-c}$ , the displacement in the strain-softening region can be solved:

$$u_c = \left[ \frac{u^{s-c} - \epsilon_r^{s-c} R_c}{\beta_c + 1} \right] \left( \frac{R_c}{r} \right)^{\beta_c} + \frac{(\epsilon_r^{s-c} + \beta_c \epsilon_\theta^{s-c}) r}{\beta_c + 1} \quad (29)$$

Combining Equations (5) and (29), the strains in the crushed region can be deduced:

$$\begin{cases} \epsilon_{rc} = \frac{\beta_c(\epsilon_r^{s-c} - \epsilon_\theta^{s-c})}{\beta_p + 1} \left( \frac{R_c}{r} \right)^{\beta_s+1} + \frac{\epsilon_r^{s-c} + \beta_c \epsilon_\theta^{s-c}}{\beta_d + 1} \\ \epsilon_{\theta c} = \frac{\epsilon_\theta^{s-c} - \epsilon_r^{s-c}}{\beta_c + 1} \left( \frac{R_c}{r} \right)^{\beta_c+1} + \frac{\epsilon_r^{s-c} + \beta_c \epsilon_\theta^{s-c}}{\beta_c + 1} \end{cases} \quad (30)$$

By substituting Equations (2) and (7) into Equation (4), the differential equation for radial stress in the crushed region can be obtained:

$$\frac{d\sigma_r}{dr} + \frac{(1 - M)\sigma_r - N_d}{r} - \frac{\eta F}{r} = 0 \quad (31)$$

When  $r = R_0$  and  $\sigma_{rd} = P_i$ , the stresses in the crushed region can be derived:

$$\begin{cases} \sigma_{rc} = \left( p_i - \frac{N_c + \eta F}{1 - M} \right) \left( \frac{R_0}{r} \right)^{1-M} + \frac{N_c + \eta F}{1 - M} \\ \sigma_{\theta c} = M \left( p_i - \frac{N_c + \eta F}{1 - M} \right) \left( \frac{R_0}{r} \right)^{1-M} + \frac{MN_c + \eta F}{1 - M} \end{cases} \quad (32)$$

### 3.4. Radii of Strain-Softening and Crushed Regions

When  $r = R_c$  and  $\sigma_{rs} = \sigma_{rc}$ , combining Equations (26) and (33), we can obtain

$$\left(\sigma_r^{e-s} - \frac{N_e + \eta F}{1 - M}\right) \left(\frac{R_s}{R_c}\right)^{1-M} + \frac{N_e - \eta F}{1 - M} + \frac{4 \cos \varphi / (\sqrt{3} - 2 \sin \varphi) \alpha (\varepsilon_\theta^{e-s} - \varepsilon_r^{e-s})}{(\beta_s + 1)(\beta_s + M)} \left[\left(\frac{R_s}{R_c}\right)^{1-\beta_s} - \left(\frac{R_s}{R_c}\right)^{1-M}\right] + \frac{4 \cos \varphi / (\sqrt{3} - 2 \sin \varphi) \alpha (\varepsilon_\theta^{e-s} - \varepsilon_r^{e-s})}{(\beta_s + 1)(1 - M)} \left[1 - \left(\frac{R_s}{R_c}\right)^{1-M}\right] = \left(p_i - \frac{N_c + \eta F}{1 - M}\right) \left(\frac{R_0}{R_c}\right)^{1-M} + \frac{N_c + \eta F}{1 - M} \tag{33}$$

Based on Equation (23), the cohesion at  $r = R_c$  can be deduced:

$$c_c = c_0 - \frac{\alpha (\varepsilon_\theta^{e-s} - \varepsilon_r^{e-s})}{\beta_s + 1} \left[ \frac{\varepsilon_\theta^{e-s} - \varepsilon_r^{e-s}}{\beta_s + 1} \left(\frac{R_s}{r}\right)^{2(\beta_s + 1)} + \frac{2\varepsilon_r^{e-s} + (\beta_s - 1)\varepsilon_\theta^{e-s}}{\beta_s + 1} \left(\frac{R_s}{r}\right)^{\beta_s + 1} - \frac{\varepsilon_r^{e-s} + \beta_s \varepsilon_\theta^{e-s}}{\beta_s + 1} \right] \tag{34}$$

Combining Equations (33) and (34),  $R_s$  and  $R_c$  can be obtained by an iterative method. The flowchart of the above calculation can be shown in Figure 5.

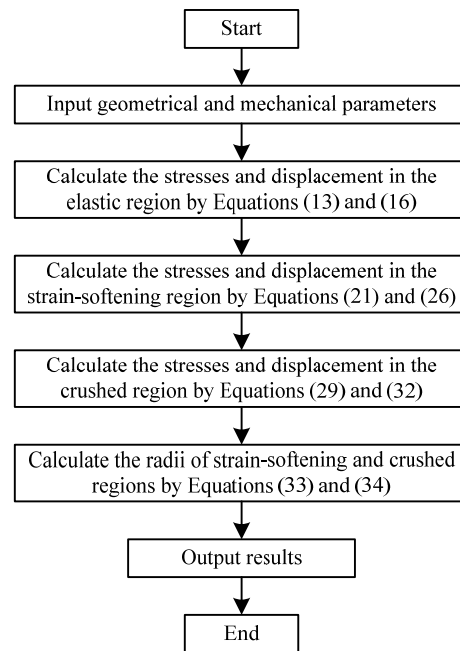


Figure 5. Flowchart of the calculation.

#### 4. Special Cases Discussion

##### 4.1. Kastner’s Formula

When  $\alpha = 0$ ,  $\psi_s = \psi_c = 0$ ,  $c_0 = c_c$ ,  $d \eta = 0$ , the current nonlinear strain-softening model degenerates for the elastic–perfectly plastic model, and the radius of the plastic region can be determined by the following equation:

$$R_s = R_0 \left( \frac{(2\sigma_0 - N_e)/(1 + M) - N_e/(1 - M)}{P_i - N_e/(1 - M)} \right)^{1/(M-1)} \tag{35}$$

Equation (35) is Kastner’s formula [15].

##### 4.2. Wilson’s Formula

When  $\alpha = \infty$ ,  $\psi_s = \psi_c = 0$ , and  $\eta = 0$ , the current nonlinear strain-softening model degenerates for the elastic–brittle-plastic model, and the radius of the plastic region can be determined by the following equation:

$$R_s = R_0 \left( \frac{(2\sigma_0 - N_e)/(1 + M) - N_c/(1 - M)}{P_i - N_c/(1 - M)} \right)^{1/(M-1)} \tag{36}$$

Equation (36) is Wilson’s formula [16].

### 5. Parameter Sensitivity Analysis

As shown in Figure 6, taking the main return laneway in Qingdong Coal Mine in Anhui Province, China, as an example, the influence of some important factors on the stresses and deformations is discussed next. The geometrical and mechanical parameters are as follows:  $R_0 = 3\text{ m}$ ,  $\sigma_0 = 18.9\text{ MPa}$ ,  $P_i = 0.4\text{ MPa}$ ,  $P_0 = 4\text{ MPa}$ ,  $\eta = 1$ ,  $R_e/R_0 = 20$ ,  $\mu = 0.25$ ,  $E = 2550\text{ MPa}$ ,  $c_0 = 4.5\text{ MPa}$ ,  $c_c = 1.1\text{ MPa}$ ,  $\varphi = 26^\circ$ ,  $\psi_s = \psi_c = 10^\circ$ , and  $\alpha = 3 \times 10^4\text{ MPa}$ .

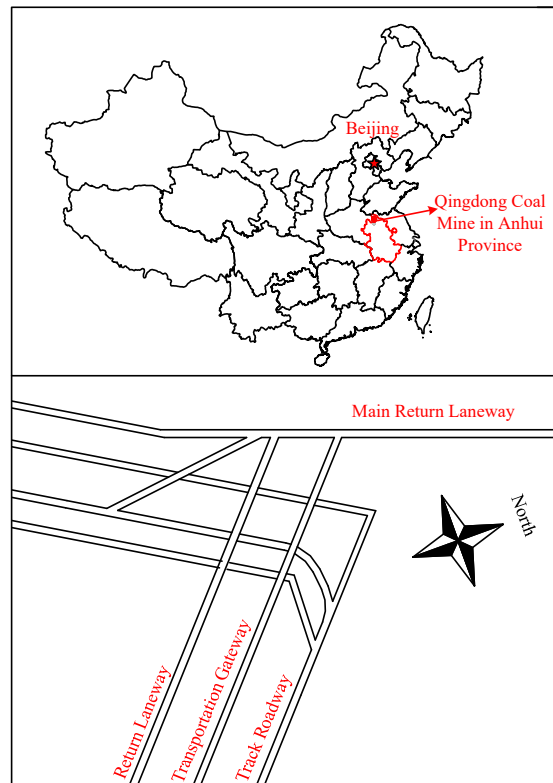


Figure 6. Location of the main return laneway.

#### 5.1. Seepage Force

Figure 7 shows the effect of seepage force on the radii of strain-softening and crushed regions and surface displacement around the tunnel. It can be seen that the  $R_s$ ,  $R_c$ , and  $u_0$  values all increase with the increasing  $P_0$ . For example, as  $P_0$  increases from 3.0 MPa to 6.0 MPa, the  $R_s$ ,  $R_c$ , and  $u_0$  increase by 1.61 m, 1.45 m, and 0.14 m, with an increment of 32.07%, 37.21%, and 91.98%, respectively. Therefore, the larger seepage force will aggravate the deformation of the tunnel.

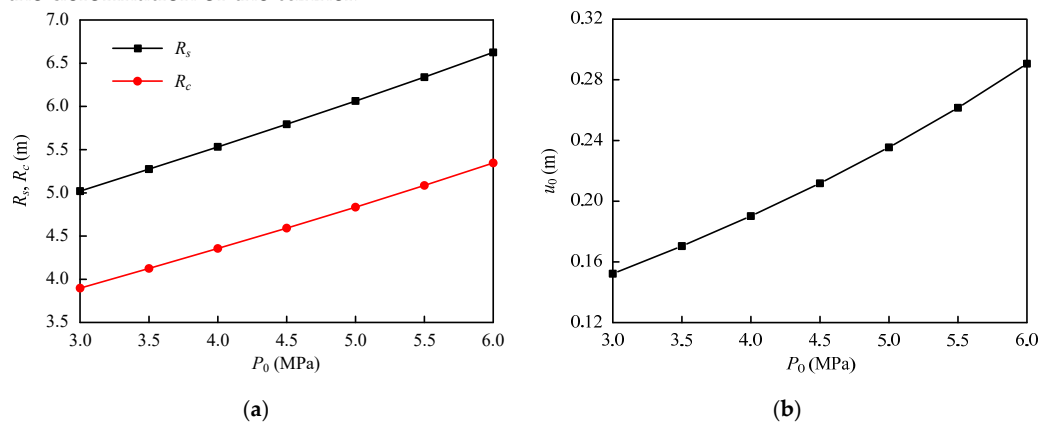


Figure 7. Effect of seepage force on the radii of strain-softening and crushed regions and surface displacement. (a)  $R_s$  and  $R_c$ ; (b)  $u_0$ .

The radial and tangential stresses in the tunnel surrounding rock with different seepage forces are shown in Figure 8. It can be seen that the radial stress is always less than the tangential stress. The radial stress at the tunnel wall is consistent with the initial support resistance, and it presents an increasing trend with the increase in radius. The tangential stress first increases in the broken and strain-softening regions and then decreases in the elastic region, and the peak value of tangential stress appears at the interface between elastic and strain-softening regions. The peak value of tangential stress increases with the increase in seepage force. For example, as the  $P_0$  value increases from 3.0 MPa to 6.0 MPa, the peak value of tangential stress increase by 6.88 MPa, with an increment of 16.95%.

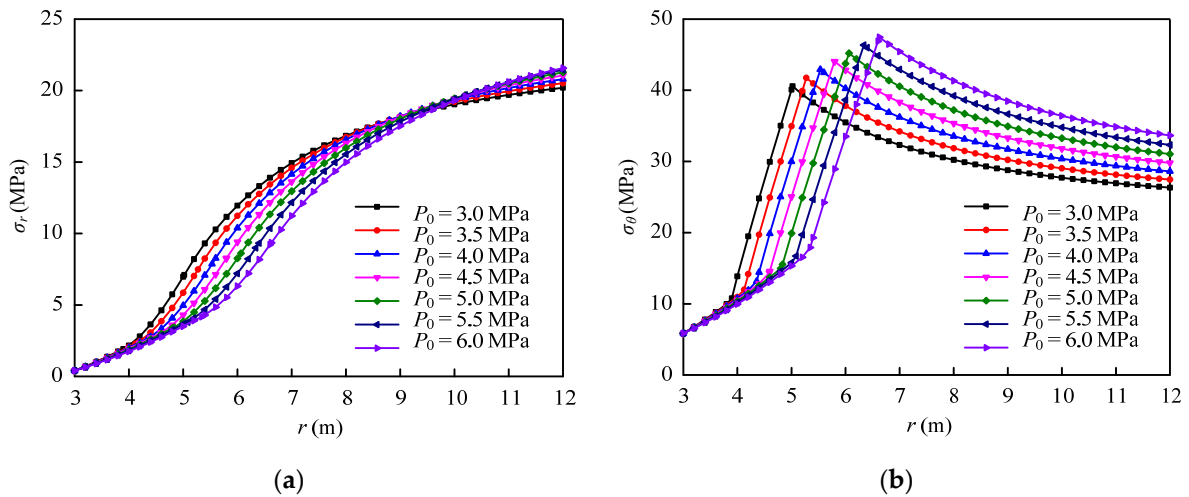


Figure 8. Effect of seepage force on the stress distribution in the tunnel surrounding rock. (a)  $\sigma_r$ ; (b)  $\sigma_\theta$ .

5.2. Softening Modulus Coefficient of Cohesion

The effect of softening modulus coefficient of cohesion on the radii of strain-softening and crushed regions and surface displacement around the tunnel is shown in Figure 9. It can be seen that the radii of strain-softening and crushed regions both increase with the increase in softening modulus coefficient. However, the ratio of the radii of the above two regions is getting smaller with the increasing softening modulus coefficient. For example, as  $\alpha$  increases from  $3 \times 10^4$  MPa to  $8.0 \times 10^4$  MPa, the ratio of  $R_s$  to  $R_c$  decreases from 1.27 to 1.13, with a reduction of 11.02%. The surface displacement also decreases with the increase in softening modulus coefficient. For example, the surface displacement is 0.19 m when the softening modulus coefficient is  $3 \times 10^4$  MPa, and surface displacement reduces to 0.18 m when the softening modulus coefficient reaches  $8 \times 10^4$  MPa.

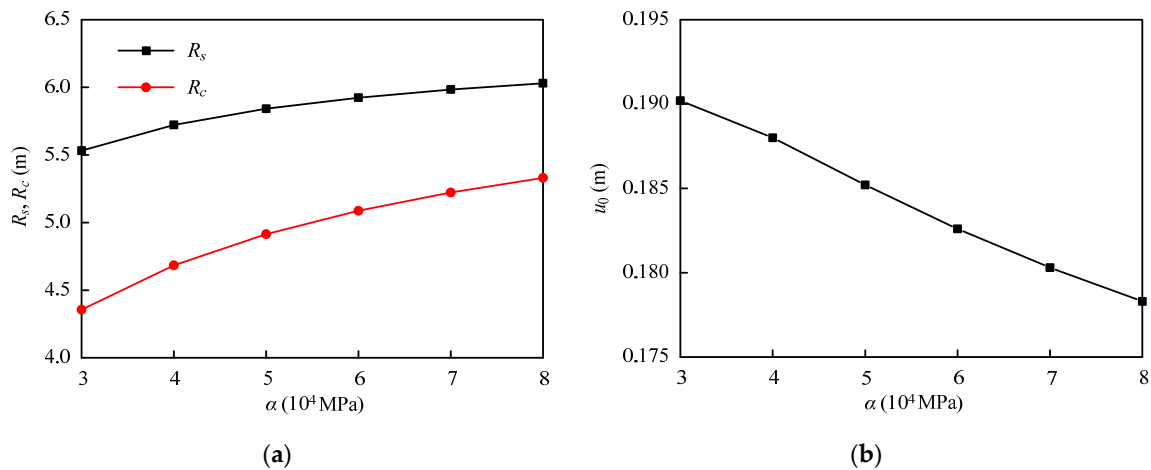


Figure 9. Effect of softening modulus coefficient of cohesion on the radii of strain-softening and crushed regions and surface displacement. (a)  $R_s$  and  $R_c$ ; (b)  $u_0$ .

The radial and tangential stresses in the tunnel surrounding rock with different softening modulus coefficients of cohesion are shown in Figure 10. It can be seen that the tangential stress is always larger than the radial stress. As the distance from the tunnel center increases, the radial stress continues to increase, and the tangential stress first increases in the crushed and strain-softening regions and then decreases in the elastic region, which is similar to the laws in Figure 8. However, the radial and tangential stresses in the crushed region are very close under different softening modulus coefficients of cohesion. Additionally, as the softening modulus coefficient increases, the peak value of tangential stress does not change, which means the sensitivity of softening modulus coefficient to stress distribution is quite low.

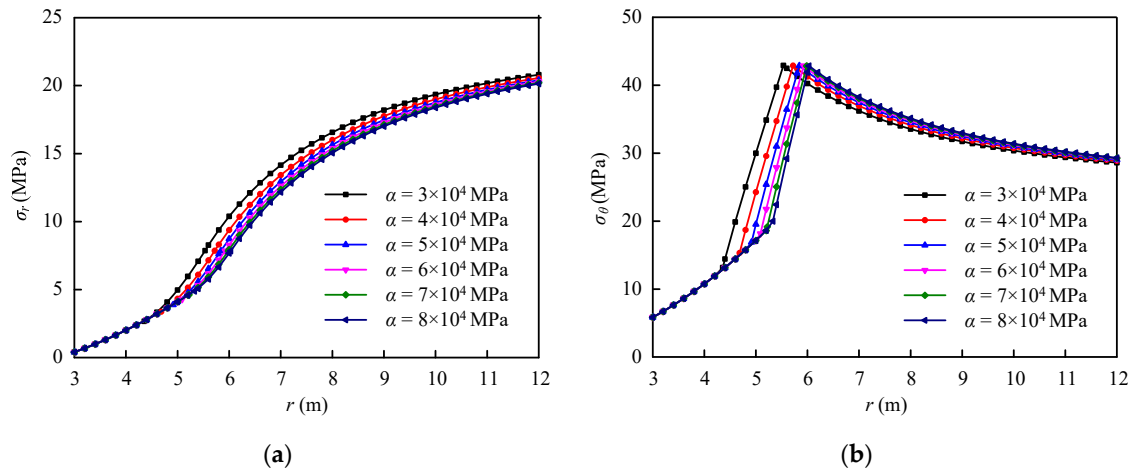


Figure 10. Effect of softening modulus coefficient of cohesion on the stress distribution in the tunnel surrounding rock. (a)  $\sigma_r$ ; (b)  $\sigma_\theta$ .

### 5.3. Initial Support Resistance

Figure 11 shows the effect of initial support resistance on the radii of strain-softening and crushed regions and surface displacement around the tunnel. It can be seen that the  $R_s$ ,  $R_c$ , and  $u_0$  values all decrease with the increasing  $P_i$ . For example, as the  $P_i$  value increases from 0 to 1.0 MPa, the  $R_s$ ,  $R_c$ , and  $u_0$  values decrease by 1.26 m, 0.99 m, and 0.09 m, with a reduction of 20.49%, 20.45%, and 38.51%, respectively. Therefore, the larger initial support resistance can control the deformation of the tunnel. As a result, some support measures, such as concrete lining and bolts, can be used to increase the initial support resistance and ensure the stability of the tunnel.

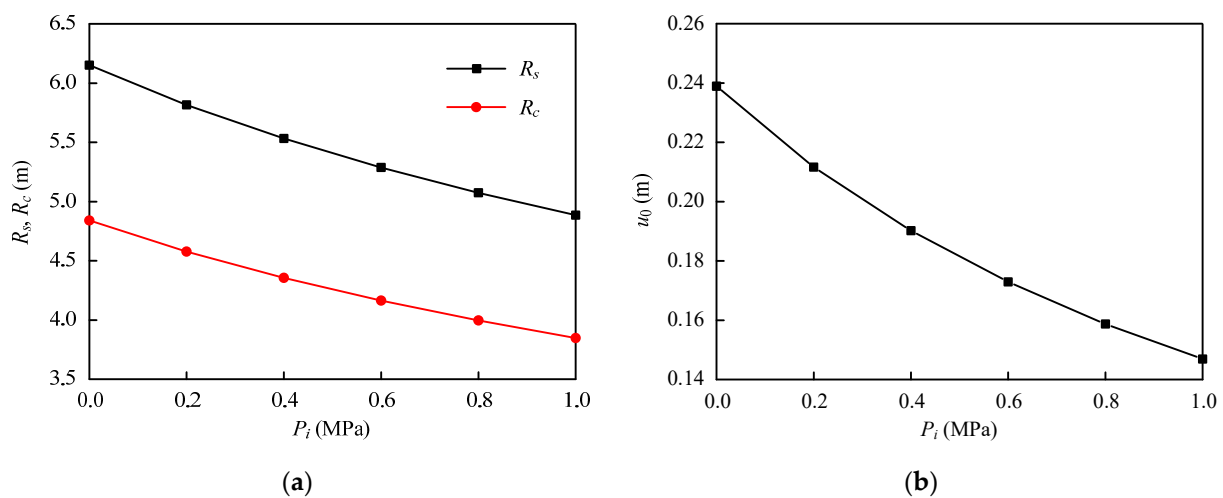
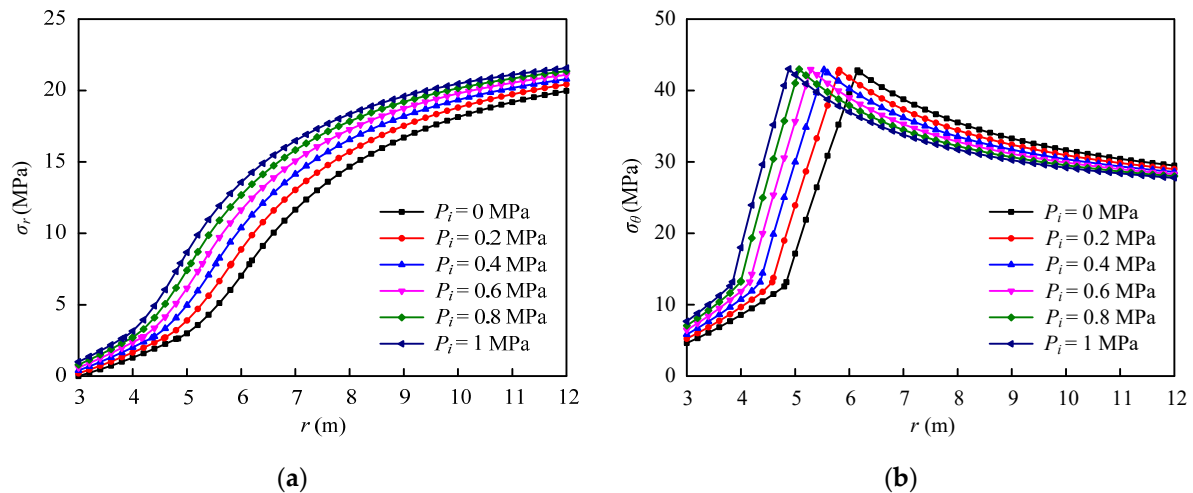


Figure 11. Effect of initial support resistance on the radii of strain-softening and crushed regions and surface displacement. (a)  $R_s$  and  $R_c$ ; (b)  $u_0$ .

The radial and tangential stresses in the tunnel surrounding rock based on different initial support resistance are shown in Figure 12. It can be seen that with the increase in initial support resistance, the whole radial stress and the tangential stress in the crushed and strain-softening regions increases while the tangential stress in the elastic region decreases. However, the peak value of tangential stress remains constant as the initial support resistance changes.



**Figure 12.** Effect of initial support resistance on the stress distribution in the tunnel surrounding rock. (a)  $\sigma_r$ ; (b)  $\sigma_\theta$ .

## 6. Conclusions

Considering the influence of seepage force, a closed-form solution for the stress distribution and deformations around the tunnels in the water area is deduced based on the new nonlinear strain-softening model. Moreover, the effects of seepage force, softening modulus coefficient of cohesion, and initial support resistance on the stress distribution, radii of the post-peak zone, and surface displacement are also discussed. The conclusions can be summarized as follows:

- (1) Compared with other solutions, when the softening modulus coefficient of cohesion and seepage force coefficient are both zero, the current solution degenerates for the elastic–perfectly plastic solution by Kastner. When the softening modulus coefficient of cohesion is large enough, and the seepage force coefficient is zero, the current solution degenerates for the elastic–brittle–plastic solution by Wilson.
- (2) The tangential stress is always larger than the radial stress. As the distance from the tunnel center increases, the radial stress continues to increase, and the tangential stress first increases in the broken and strain-softening regions and then decreases in the elastic region. The peak value of tangential stress appears at the interface between elastic and strain-softening regions.
- (3) As the seepage force increases, the radii of strain-softening and crushed regions and surface displacement all increase. As the softening modulus coefficient of cohesion increases, the radii of strain-softening and crushed regions increase while the surface displacement decreases. Additionally, the radii of strain-softening and crushed regions and surface displacement all decrease with the increasing initial support resistance.

This study only analyzes the stresses and deformations of tunnels through theoretical methods. Further research on numerical simulation should be carried out in the future.

**Author Contributions:** Conceptualization, H.F. and L.W.; methodology, H.F.; validation, L.W. and S.L.; formal analysis, H.F.; resources, S.L.; data curation, S.L.; writing—original draft preparation, H.F.; writing—review and editing, L.W.; supervision, S.L.; funding acquisition, L.W. All authors have read and agreed to the published version of the manuscript.

**Funding:** This study is supported by the Scientific Research Foundation for High-level Talents of Anhui University of Science and Technology (No. 2021yjrc15), Major Special Projects of Science and Technology of Anhui Province (No. 202203a07020010), Collaborative Innovation Project of Anhui Province (GXXT-2020-055), and Opening Foundation of the State Key Laboratory of Mining Response and Disaster Prevention and Control in Deep Coal Mines (No. SKLMRDPC21KF09).

**Data Availability Statement:** The data used for conducting classifications are available from the corresponding author upon request.

**Acknowledgments:** The authors would like to thank the engineers in Qingdong Coal Mine for their engineering data.

**Conflicts of Interest:** The authors declare no conflict of interest.

## References

1. Detournay, E. Elastoplastic model of a deep tunnel for a rock with variable dilatancy. *Rock Mech. Rock Eng.* **1986**, *19*, 99–108. [[CrossRef](#)]
2. González-Cao, J.; Varas, F.; Bastante, F.G.; Alejano, L.R. Ground reaction curves for circular excavations in non-homogeneous, axisymmetric strain-softening rock masses. *J. Rock Mech. Geotech. Eng.* **2013**, *5*, 431–442. [[CrossRef](#)]
3. Luo, Y.; Gong, F.Q.; Zhu, C.Q. Experimental investigation on stress-induced failure in D-shaped hard rock tunnel under water-bearing and true triaxial compression conditions. *Bull. Eng. Geol. Environ.* **2022**, *81*, 76. [[CrossRef](#)]
4. Liang, R.Z.; Wu, J.; Sun, L.W.; Shen, W.; Wu, W.B. Performances of adjacent metro structures due to regional excavation of a large-scale basement in soft ground. *Tunn. Undergr. Space Technol.* **2021**, *117*, 104123. [[CrossRef](#)]
5. Tonon, R.C.F. Closed-form solutions for a circular tunnel in elastic-brittle-plastic ground with the original and generalized Hoek–Brown failure criteria. *Rock Mech. Rock Eng.* **2011**, *44*, 169–178.
6. Lv, A.; Masoumi, H.; Walsh, S.D.C.; Roshan, H. Elastic-Softening-Plasticity around a borehole: An analytical and experimental study. *Rock Mech. Rock Eng.* **2019**, *52*, 1149–1164. [[CrossRef](#)]
7. Carranza-Torres, C. Elasto-plastic solution of tunnel problem using the generalized form of the Hoek-Brown failure criterion. *Int. J. Rock Mech. Min.* **2004**, *41*, 480–481. [[CrossRef](#)]
8. Hao, Y.; Wu, Y.; Mao, X.; Li, P.; Zhang, L.; Tao, J. An elastoplastic softening damage model for hydraulic fracturing in soft coal seams. *Adv. Civ. Eng.* **2018**, *2018*, 2548217. [[CrossRef](#)]
9. Park, K.H.; Tontavanich, B.; Lee, J.G. A simple procedure for ground response curve of circular tunnel in elastic-strain softening rock masses. *Tunn. Undergr. Space Technol.* **2008**, *23*, 151–159. [[CrossRef](#)]
10. Pourhosseini, O.; Shabanimashcool, M. Development of an elasto-plastic constitutive model for intact rocks. *Int. J. Rock Mech. Min. Sci.* **2014**, *66*, 1–12. [[CrossRef](#)]
11. Brown, E.; Bray, J.; Ladanyi, B.; Hoek, E. Ground response curves for rock tunnels. *J. Geotech. Eng.* **1983**, *109*, 15–39. [[CrossRef](#)]
12. Masoudian, M.S.; Hashemi, M.A. Analytical solution of a circular opening in an axisymmetric elastic-brittle-plastic swelling rock. *J. Nat. Gas Sci. Eng.* **2016**, *35*, 483–496. [[CrossRef](#)]
13. Sharan, S.K. Elastic-brittle-plastic analysis of circular openings in Hoek-Brown media. *Int. J. Rock Mech. Min.* **2003**, *40*, 817–824. [[CrossRef](#)]
14. Zareifard, M.; Fahimifar, A. Analytical solutions for the stresses and deformations of deep tunnels in an elastic-brittle-plastic rock mass considering the damaged region. *Tunn. Undergr. Space Technol.* **2016**, *58*, 186–196. [[CrossRef](#)]
15. Kastner, H. *Statik des Tunnel-Und Stollenbaues*; Springer: New York, NY, USA, 1962.
16. Wilson, A.H. A method of estimating the closure and strength of lining required in drivages surrounded by a yield zone. *Int. J. Rock Mech. Min. Geomech. Abstr.* **1980**, *17*, 349–3550. [[CrossRef](#)]
17. Ghorbani, A.; Hasanzadehshooiili, H.; Sadowski, L. Neural prediction of tunnels' support pressure in elasto-plastic, strain-softening rock mass. *App. Sci.* **2018**, *8*, 841. [[CrossRef](#)]
18. Han, J.X.; Li, S.C.; Li, S.C.; Yang, W.M. A procedure of strain-softening model for elasto-plastic analysis of a circular opening considering elasto-plastic coupling. *Tunn. Undergr. Space Technol.* **2013**, *37*, 128–134. [[CrossRef](#)]
19. Li, Y.; Cao, S.; Fantuzzi, N.; Liu, Y. Elastoplastic analysis of a circular borehole in elastic-strain softening coal seams. *Int. J. Rock Mech. Min.* **2015**, *80*, 316–324. [[CrossRef](#)]
20. Wang, S.L.; Yin, X.T.; Tang, H.; Ge, X. A new approach for analyzing circular tunnel in strain-softening rock masses. *Int. J. Rock Mech. Min.* **2010**, *47*, 170–178. [[CrossRef](#)]
21. Jing, W.; Xue, W.; Yao, Z. Variation of the internal friction angle and cohesion of the plastic softening region rock in roadway surrounding rock. *J. China Coal Soc.* **2018**, *43*, 2203–2210.
22. Lu, Y.; Wang, L.; Yang, F.; Li, Y.; Chen, H. Post-peak strain softening mechanical properties of weak rock. *Chin. J. Rock Mech. Eng.* **2010**, *29*, 640–648.
23. Fahimifar, A.; Ghadami, H.; Ahmadvand, M. The influence of seepage and gravitational loads on elastoplastic solution of circular tunnels. *Sci. Iran.* **2014**, *21*, 1821–1832.
24. Fahimifar, A.; Zareifard, M.R. A theoretical solution for analysis of tunnels below groundwater considering the hydraulic-mechanical coupling. *Tunn. Undergr. Space Technol.* **2009**, *24*, 634–646. [[CrossRef](#)]

25. Huangfu, M.; Wang, M.S.; Tan, Z.S.; Wang, X.Y. Analytical solution for steady seepage into an underwater circular tunnel. *Tunn. Undergr. Space Technol.* **2010**, *25*, 391–396. [[CrossRef](#)]
26. Fan, H.; Wang, L.G.; Wang, S.; Jiang, C.Y. A new unified solution for deep tunnels in water-rich areas considering seepage force. *Geofluids* **2021**, *2021*, 6696757. [[CrossRef](#)]
27. Mogi, K. Flow and fracture of rocks under general triaxial compression. *Appl. Math. Mech.* **1981**, *2*, 635–651. [[CrossRef](#)]

**Disclaimer/Publisher’s Note:** The statements, opinions and data contained in all publications are solely those of the individual author(s) and contributor(s) and not of MDPI and/or the editor(s). MDPI and/or the editor(s) disclaim responsibility for any injury to people or property resulting from any ideas, methods, instructions or products referred to in the content.